RSC Advances

PAPER

CrossMark
← click for updates

Water soluble blue-emitting AuAg alloy nanoparticles and fluorescent solid platforms for removal of dyes from water†

Srikrishna Pramanik, Arindam Saha and Parukuttyamma Sujatha Devi*

Chicken egg shell membrane, a naturally abundant protein membrane, was used to synthesize gold (Au), silver (Ag) and their bimetallic (AuAg) alloy nanoclusters at room temperature without the use of any reducing agent or catalyst. The as-formed gold and alloy clusters were highly fluorescent and exhibited intense blue emission around 435 ± 5 and 440 ± 5 nm, respectively. This is the first report confirming the formation of fluorescent alloy clusters exhibiting nanosecond lifetimes by a biomembrane-induced reduction process. We have also explored the capability of these metal cluster immobilized inexpensive ESMs in removing organic dyes from water. The results confirmed that it is the strong adsorption of the dye molecules in the presence of the metal particles that has helped to convert ESM into an effective platform for water purification. This process has the dual advantages of utilizing an inexpensive, abundant and eco-friendly food waste (egg shell membrane) for *in situ* reduction and formation of metal nanoparticles and the utilization of the same as an effective platform for the removal of anionic dyes from waste water. An Au-immobilized ESM showed a better efficiency in dye molecules removal than those of the Ag-ESM and AuAg-ESM membranes.

1. Introduction

Noble metal nanoparticles and their alloy clusters are important in many areas, such as medical diagnosis, controlled drug delivery, sensors and catalysis.[1,2] Although a large number of methods are currently available for the preparation of metal/alloy nanoparticles, so far environmentally friendly techniques have been poorly explored for this purpose. The current interest, therefore, has been focused on exploring environment-friendly synthetic approaches for preparing fluorescent alloy nanoparticles/clusters for various applications. Several groups have explored protein-based synthesis to produce stable fluorescent nanomaterials for applications in bioimaging,[3] biosensing[4] and metal ion detection.[5] Xie *et al.* synthesized highly fluorescent Au nanoclusters (AuNCs) exhibiting red emission using bovine serum albumin (BSA),[6] whereas Guo and Irudayaraj synthesized fluorescent Ag clusters using BSA[7] and

Singh *et al.* demonstrated the synthesis of Au, Ag, and AuAg alloy nanoparticles using BSA as a reducing and foaming agent.[8] Liu *et al.* reported the direct synthesis of fluorescent gold nanoclusters using insulin as a template.[9] Mohanty *et al.* reported the synthesis of luminescent AuAg alloy clusters of quantum size using a protein template.[10] Gui and Jin used human serum albumin (HSA) to prepare AuAg core shell nanocrystals.[11] Recently, we explored the use of egg shell membrane (ESM), a naturally occurring biotemplate, to prepare fluorescent gold nanoparticles.[12] ESM has a 3D entangled structure of highly cross-linked fibres and porous sites. The super abundant, economically benign character and unique features make ESM superior to other naturally available proteins like bovine serum albumin, human serum albumin, *etc.* The ESM is insoluble in water due to the presence of a large number of cross-linked disulphide bonds.[13] The ESM mainly consists of glycoprotein-like collagen (types I, V and X) and several other amino acids, mainly glycine, cysteine, uronic acid, *etc.*[14–16] On the other hand, the presence of amino acids makes ESM a good reducing agent and stabilizer. In recent times many research groups have used ESM to prepare AgNPs, AuNPs and other oxide materials.[12,13,17–19] The metal NP immobilized ESM has shown unique advantages in biosensing,[20] surface-enhanced Raman spectroscopy[21] and in catalysis.[22,23] The ESM can also act as a platform to retrieve heavy toxic metal ions, such as arsenic and mercury, from water.[24] Here, we demonstrate the simultaneous *in situ* reduction of Au and Ag ions by ESM resulting in the formation of highly fluorescent AuAg alloy

Nano-Structured Materials Division, CSIR-Central Glass and Ceramic Research Institute, 196, Raja SC Mullick Road, Jadavpur, Kolkata 700032, India. E-mail: psujathadevi@cgcri.res.in; psujathadevi@gmail.com; Fax: +91-33-2473-0957; Tel: +91-033-2483-8082

† Electronic supplementary information (ESI) available: *In situ* formation of metal nanoclusters by UV-Vis data, emission data of fluorescent AuNCS, and alloy NCs, DLS and zeta potential data, EDAX and HRTEM data on the synthesized nanoparticles, UV-Vis data depicting the interaction of membranes with MO dye in buffer solution, MV dye in distilled water and interaction of AuAg nanoclusters with MO dye, and desorption experiments. See DOI: 10.1039/c4ra14176h

nanoparticles and metal ion immobilized fluorescent solid ESM platforms. In addition, we also demonstrate the unique dye-adsorbing capability of these metal ion immobilized ESM platforms for the efficient removal of anionic dyes from waste water at room temperature. The novelty of this technique lies in the unique properties of these protein membranes since they are highly resistant to pH, safe to handle, and abundantly available in nature.[13]

2. Experimental section

2.1 Materials

AR grade chloroauric acid (HAuCl$_4$, S.D. Fine-Chem. Ltd, India), silver nitrate (S.D. Fine-Chem. Ltd, India), Methyl Orange (Sigma-Aldrich Chemicals) and phosphate buffer (Merck India) were used for the experiments. All reagents were used as received without further purification.

2.2 Synthesis

The cleaned egg shells were treated with dilute acetic acid (50% diluted with water) to extract the membrane (ESM) from the egg shell by soaking them for 4–6 hours. Once the calcium carbonate shell dissolved, the membranes were carefully collected and thoroughly washed with deionized water and then dried in air at room temperature. For the synthesis of Au and Ag nanoparticles, 0.150 g of ESM was added to 10 ml of the individual metal ion solutions (10^{-2} M) and the reaction allowed to proceed at room temperature in the dark. For the synthesis of alloy nanoparticles, extracted dried ESM (0.150 g) was added to a mixed solution of 5 ml of AgNO$_3$ and 5 ml of HAuCl$_4$, each of 10^{-2} M, and the reaction allowed to proceed at room temperature. The concentration of the metal ions used was varied from 10^{-2} M to 10^{-3} M and the exposure time for the reaction was extended up to seven days. In the manuscript NC represents nanoclusters and NP represents nanoparticles.

2.3 Characterization

The absorption spectra were measured on a SHIMADZU UV-3600 UV-Vis-NIR spectrophotometer. The solution was taken out from the impregnated membrane from time to time for seven days and the absorbance was recorded at regular intervals of time. The fluorescence spectra of the same solutions were recorded at room temperature on a Steady State Spectro-fluorometer (QM-40, Photon Technology International, PTI) equipped with a 150 Watt Xenon lamp as an excitation source. The emission spectra of the solution were recorded by exciting at 340 nm using a fixed excitation and emission band pass of 5 nm. Raman spectra were obtained using a Renishaw inVia Reflex micro Raman spectrometer with an argon ion (785 nm) laser. The spectra were collected at a resolution of 1 cm^{-1}. The room temperature powder X-ray diffraction (XRD) was carried out on the immobilized membranes for phase identification using a Philips X-ray diffractometer (PW1730) with CuKα radiation at a 2θ scan rate of 2° per minute. For the Raman and XRD experiments, metal nanoparticle immobilized ESMs were cut into square pieces and pasted on thin glass plates. The

transmission electron microscopy (TEM) images were taken on a TECNAI G^2 30 high-resolution transmission electron microscope operating at 300 kV. For the TEM study a few drops of the colloidal nanoparticles were deposited on the carbon coated Cu grid and dried under an IR lamp. Field emission scanning electron micrographs (FESEM) were carried out in a Field Emission Scanning Electron Microscope (SUPRA™ 35 VP; Gemini Column (Carl Zeiss SMT)). Time-correlated single photon counting (TCSPC) measurements were performed on the water dispersions with a Horiba Jobin Yvon IBH Fluorocube apparatus after exciting the sample with a 340 nm excitation lamp. The fluorescence decay was collected with a Hamamatsu MCP (R3809) photomultiplier at 435 nm, and the fluorescence decay was analysed with IBH DAS6 software. The particle size and zeta potential of the dispersions were measured on a HORIBA (SZ-100 OZ) dynamic light scattering particle size analyser.

2.4 Dye adsorption experiment

In order to carry out the dye adsorption studies, 10 mg of metal nanoparticle immobilized ESM (Au-ESM, Ag-ESM, AuAg-ESM) were added to 10 ml of 10^{-5} M Methyl Orange (MO) solution, and placed in separate culture tubes covered with aluminium foil and kept in the dark. The dye adsorption experiment was also performed in a phosphate buffer solution at a pH of 7.00 using AuAg-ESM and the dye adsorption characteristics monitored. The pH of the solution remained almost the same after the addition of the membrane to the solution. The adsorption characteristics of the MO dye were monitored by recording the absorbance of the dye solution (λ_{max} at 464 nm) from time to time at various time intervals. The % of dye removed from solution was calculated as shown in eqn (1).

$$\% \text{ of dye removed} = \frac{C_0 - C_t}{C_0} \times 100 \qquad (1)$$

where C_0 is the initial concentration of dye, and C_t is the concentration of dye at various time intervals. Here C_0 is equivalent to A_0, the initial absorbance, and C_t is equivalent to A_t, the absorbance recorded at different times, where $A = \varepsilon CL$, where ε is the molar extinction coefficient and L is the path length of the monochromatic light.

## 3. Results and discussion

3.1 Optical studies

To gain insight about the reduction process and subsequent particle formation, the *in situ* reactions were continuously monitored by the absorbance and fluorescence spectral changes during the course of the reaction. The initial studies were carried out with gold and silver and subsequently the study was extended to the gold silver alloy system. The spectral changes during the interaction of ESM with different concentrations of HAuCl$_4$ and AgNO$_3$ are shown in the (ESI Fig. S1 and S2,† respectively). The formation of Au and Ag nanoclusters was confirmed by the characteristic surface plasmon resonance (SPR) bands in the UV-Vis spectra. The spectrum recorded at

room temperature as a function of time exhibited the systematic appearance of a broad band with a maximum around 535 nm for Au and 435 nm for Ag nanoclusters. The characteristic SPR peak appeared at a λ_{max} of 535 ± 2 nm for Au nanoclusters (Fig. S1†) and in the case of Ag nanoclusters, the maximum absorbance was observed at 436 ± 2 nm (Fig. S2†).

The spectral changes observed in a typical experiment with a 1 : 1 mixture of AgNO₃ solution (10^{-2} M) and HAuCl₄ (10^{-2} M) are presented in Fig. 1a. The AuAg alloy nanoclusters displayed only a single SPR peak with a maximum absorbance at around 546 ± 3 nm (Fig. 1a). This bathochromic shift compared to bare Au (535 ± 2 nm) and Ag nanoclusters (436 ± 2 nm) gives an indication of the formation of alloy clusters of larger size than the individual metal clusters. At the end of the reaction, the SPR band intensity remained invariant, the attained saturation indicating the complete reduction of metal ions and formation of AuAg alloy clusters. In order to monitor the rate of reduction process, we plotted the change in absorbance of the alloy dispersion with time, as shown in Fig. S3.† During the course of the experiment, the mixed metal ion solution changed colour from yellow to pink, whereas the Au and Ag solutions changed to blue and brown, respectively, as can be seen from the inset of Fig. 1b. The first observation of the colour change on the membrane confirms the formation and deposition of metal

nanoclusters on the membrane. Interestingly, when the experiments were carried out with lower concentrations of the metal ions (10^{-3} M each), there was no indication of any SPR peak formation in the absorption spectra, as evident from the ESI shown in Fig. S4.† The absorption spectra of Au, Ag and the AuAg alloy dispersions shown in Fig. 1b exhibit only a single absorption band, thereby confirming the formation of alloy nanoclusters.

To verify whether the alloy nanoclusters formed in solution exhibited fluorescence, we recorded the emission spectra of the colloidal solutions of Au, Ag and AuAg clusters at room temperature. The control solution of HAuCl₄, AgNO₃ or the mixture had no visible fluorescence in the range studied (350–700 nm). Time-dependent fluorescence studies during the reduction process were monitored using a 10^{-2} M metal ion solution and the results are shown in Fig. 1c. The Au nanoclusters exhibited the characteristic blue emission around 435 ± 5 nm upon excitation at 340 nm (Fig. 1d). Interestingly, Ag nanoclusters did not exhibit any visible emission, whereas AuAg nanoclusters exhibited an intense blue emission at 440 ± 5 nm. In addition, the characteristic emissions of the Au nanoclusters at 540 nm and 720 nm, on excitation at 500 nm and 680 nm, respectively, were absent for the AuAg alloy clusters, as clear from the ESI† in Fig. S6.[12]
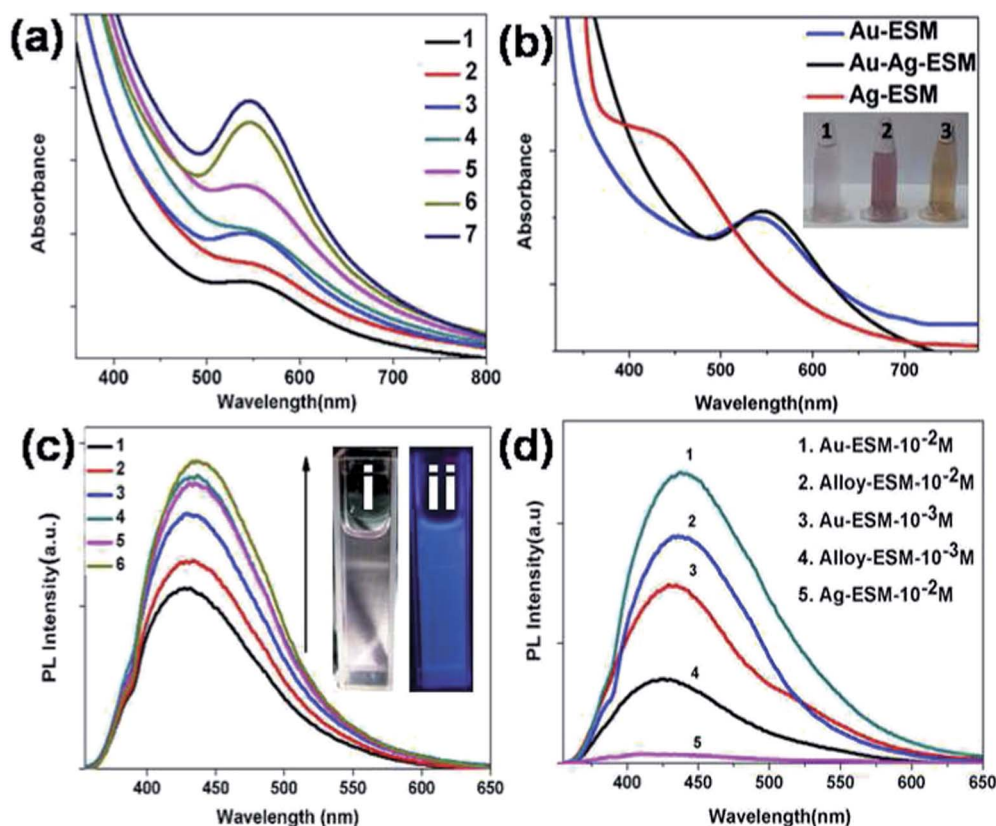
Fig. 1 (a) UV-Vis absorption spectra of the Au−Ag mixture in presence of ESM. (b) Comparison of UV-Vis spectra of the Au NPs, AuAg NPs and Ag NPs after the end of the reaction. The inset shows the image of colloidal Au (1), AuAg (2), and Ag NPs (3). (c) Fluorescence spectra of the AuAg alloy solution (10^{-2} M HAuCl₄ + 10^{-2} M AgNO₃ + ESM) at 340 nm excitation. Curves (1–6) represent the emission peak for 1–7 days. (d) The fluorescence spectra of Au, Ag and their bimetallic alloy solution at various concentrations. The inset in (c) shows the digital image of the dispersions in normal light and on exposure to UV light (blue colour).

As evident from Fig. 1d, the observed emission intensity varied with the concentration of the metal ions. The blue emission exhibited by gold clusters has been assigned to the Au 6s to 6p intraband transition. Interestingly, the emission intensity was lower for the alloy nanoclusters compared to the Au nanoclusters, probably because the doping of Ag into Au during the alloy formation resulted in quenching of the emission. Although the presence of Ag in AuAg nanoclusters quenched the emission weakly, the existence of Au in the alloy favoured the excitation of the d band electron to a higher sp level followed by recombination of the electron hole pair to give rise to the observed emission. By density functional theory, Zhang et al. have shown that Ag doping can modulate the optical properties of Au clusters.[25] Dou et al. reported aggregation between Au clusters and Ag clusters affecting the emission spectra of AuAg bimetallic nanostructures.[26] In order to further confirm that the reduction of a mixed solution of silver and gold in presence of ESM has resulted in the formation of a fluorescent alloy cluster, we measured the fluorescence of a 1:1 mechanical mixture of Au nanoclusters and Ag nanoclusters, as shown in Fig. S7.† Interestingly, the mechanical mixture did not exhibit any emission similar to that of the alloy clusters, thereby confirming the complete quenching of the emission of Au nanoclusters in the presence of Ag nanoclusters. The above result is contrary to what we have observed for the alloy clusters formed in situ, thus corroborating other results on the formation of AuAg alloy nanoclusters during the in situ reduction reaction. The digital images of the alloy dispersions in normal light (i) and on exposure to a UV light (ii) are presented in the inset of Fig. 1c.

During the course of the experiment, the mixed metal ion solution changed colour from yellow to colourless to deep pink, as can be seen from the digital images shown in Fig. 2 and the

Fig. 2 A schematic of the formation of metal nanoclusters and metal immobilized ESM.

inset of Fig. 1b. The ESM surface also displayed different colours after immobilization of the metal ions. The Au-ESM turned pink, whereas the surface of the ESM turned brown for Ag and bluish-red for AuAg, as evident from the pictures of dried membranes shown in Fig. 2. The particle distribution representing the hydrodynamic diameter measured by the DLS technique is presented in Fig. S8a.† It can be seen that the hydrodynamic diameter of the AuAg clusters (133.5 nm) is much larger compared to that of the individual metal clusters. The alloy cluster exhibited a broader distribution compared to the corresponding individual metal cluster dispersions. The zeta potential of the dispersions varied in the order +9.6, +3.8 and +8.2 mV, respectively, for Au, Ag and AuAg clusters, confirming their positively charged surface characteristics (Fig. S8b†).

Interestingly, when we carried out the emission experiments with lower concentrations of the metal ions (10^{-3} M each), both the Au nanocluster and the alloy nanocluster exhibited strong visible emissions, as evident in curves (3) & (4) of Fig. 1d. It is worth noting the absence of a strong SPR band at lower concentrations (Fig. S4†). In order to understand the effect of particle size on the optical properties, we separated the larger and smaller particles by centrifuging the as-formed dispersion (10^{-2} M) at 10 000 rpm for 20 minutes. The supernatant and the precipitates were separately characterized via absorption and emission measurements. It was found that the supernatant was mostly composed of smaller nanoclusters of average size around 36.7 nm after 3 days and 47.2 nm after 7 days as evident from the DLS data shown in Fig. S9a and d.† The precipitate, on the other hand, exhibited larger sized clusters of 84 nm after 3 days and 104 nm after 7 days, as shown in Fig. S9a and d.† In Fig. S9b and e,† the UV-Vis spectra of the smaller and larger clusters collected on the 3rd and 7th days are presented. Similarly, in Fig. S9c and f,† the emission data of the smaller and larger clusters are presented. Compared to the as-formed clusters, the separated fractions exhibited slightly different absorbance maxima of 545 ± 2 nm for the larger sized fraction and 530 ± 2 nm for the smaller sized fraction. There was not much difference in the absorbance maximum with time except a reduction in the absorbance. Interestingly, the emission maxima of all the samples remained the same. It is evident that the smaller particles exhibited a stronger emission compared to the larger particles (Fig. S9c and f†), without any shift in the peak position. The larger nanoparticles are expected to quench the fluorescence of the smaller particles and, accordingly, we noticed a reduction in the fluorescence intensity after 7 days of the reaction. It is very hard to control the invariant growth of the particles as ESM contains several amino acids with binding or reducing sites with different reducing capability, resulting in particles of variable size and shape forming various metallic clusters.

Time correlated single photon counting (TCSPC) measurements were performed by exciting the sample with a 340 nm excitation lamp. The fluorescence decay was collected at 435 nm (Fig. 3). Au nanoclusters exhibited a third order exponential decay with $\tau_1 = 2.572$ ns, $\tau_2 = 9.9$ ns and $\tau_3 = 0.3$ ns and their relative percentages were 43.82, 38.94 and 17.24, respectively.
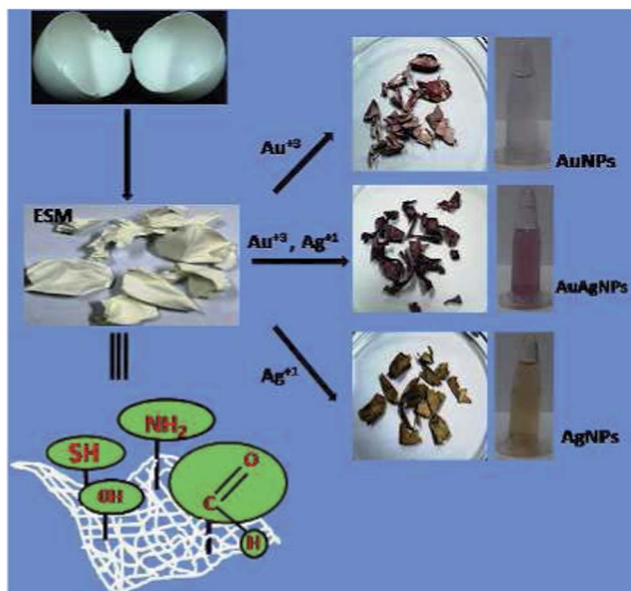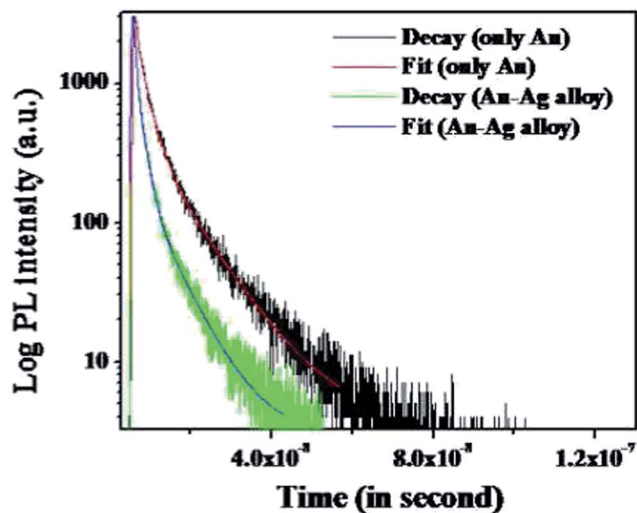
Fig. 3 Comparison of photoluminescence lifetime decay of Au and AuAg alloy nanoparticles. The alloy nanoparticles show a shorter lifetime compared to the Au nanoparticles.

From this data, it is clear that the major contribution to the average lifetime was from τ_1 and τ_2, and was around 84% of the total lifetime and both were of a nanosecond order. The AuAg alloy also exhibited third order exponential decay with $\tau_1 = 1.6$ ns, $\tau_2 = 7.1$ ns and $\tau_3 = 0.125$ ns and their relative percentages were 37.68, 22.85 and 39.47, respectively. In this case, the major contributions were from τ_1 and τ_3, and was around 76% of the total lifetime and an order less than that of Au nanoparticles. The reduced lifetime in alloy nanoclusters is caused by the incorporation of Ag in Au nanoparticles, which induces quenching of fluorescence from the Au nanoparticles, resulting in shorter lifetimes. These findings further prove the successful synthesis of AuAg alloy nanoclusters by ESM.

3.2 Morphological evaluation

The exact particle size and morphology of the synthesized nanoparticles were monitored using transmission electron microscopy (TEM). In Fig. 4a–c, typical bright-field images of Au, Ag and AuAg alloy nanoclusters are presented. A typical image of the Au colloidal solution (Fig. 4a) shows the presence of a large number of spherical and triangular particles of size smaller than 50 nm. The silver particles of size within 5–20 nm, on the other hand, grew and assembled into islands of flowers, as shown in Fig. 4b. Most of the alloy particles were spherical or elongated in shape (Fig. 4c). In Fig. 4d–f, the particle size distribution generated from the TEM images using image j software is presented. The distributions of particles were within 5–50 nm for Au, 3–30 nm for Ag and 5–100 nm for AuAg. The average size distribution from the TEM images (Fig. 4d–f) shows average sizes of 18.12 nm, 12.4 nm and 42.21 nm, respectively, for Au, Ag and AuAg nanoclusters. The alloy clusters are much larger in size compared to the corresponding individual metal clusters. The AuAg dispersion exhibited the presence of both larger and finer particles. High resolution transmission electron microscopic (HRTEM) images and selected area electron diffraction (SAED) patterns of the AuAg nanoparticles are shown in Fig. 4g and h, respectively. Energy dispersive X-ray analysis (EDAX) was performed on the selected particles to further confirm the presence of both Au and Ag in the alloy nanoparticles (Fig. S10†). The characteristic peaks of Au at 2.195 keV and 9.72 keV, and of Ag at 2.98 keV and 3.2 keV confirmed the presence of both gold and silver in the alloy particles.[27,28] The crystalline nature of the AuAg alloy is confirmed through the HRTEM image shown in Fig. 4g. The measured spacing between adjacent lattice fringes of 0.235 nm is compatible with the 111 reflections of Au (Fig. S11†) and Ag (Fig. S12†) with a face centred cubic structure. Au and Ag have a similar ionic radii of 1.44 Å, and hence the lattice fringes do not show much difference compared to the corresponding metal nanoparticles. The SAED pattern of AuAg alloy in Fig. 4h also confirms the successful formation of the crystalline alloy nanoparticles. The TEM image of the alloy in Fig. 4c clearly confirms the formation of clusters. In Fig. 4i, an expanded TEM picture of a single particle is shown that clearly indicates the formation of twinned nanostructures. The FCC metals like Au and Ag are known to form twinned structures. Herein, the slow reduction of the metal ions by ESM results in a slow nucleation and restricts the separate nucleation of Ag or Au and formed the twinned AuAg alloy particles.

Microstructural change and morphology of the *in situ* generated particles embedded on the Au-ESM, Ag-ESM and AuAg-ESM were characterized by FESEM at different magnifications. From the SEM images it can be clearly seen that ESM has an interlinked net-like fibre structure. In Fig. 5a and b the spherical nature of the finely deposited particles on the fibrous network of the membrane surface can be clearly seen. The EDAX spectrum recorded on the membrane confirms the presence of both Au and Ag on the solid membrane (Fig. S13†). The X-ray powder diffraction (XRD) analysis further proved the crystalline nature of the metal particles immobilized on the surface of ESM. The natural ESM was amorphous to X-rays, whereas the metal nanoparticle immobilized membranes were highly crystalline in nature, as evident from the XRD patterns shown in Fig. 5c. The AuAg-ESM exhibited characteristic diffraction peaks that corresponded to the 111 and 200 planes of the metallic particles at 2θ values of 38.37° and 44.46°, respectively. From Fig. 5c, it can be seen that the diffraction peaks are slightly shifted in the case of AuAg-ESM compared to Au-ESM and Ag-ESM. The 2θ value of the (111) plane appeared at 38.18° and 38.26°, respectively, for Au (JCPDS 04-0784) and Ag (JCPDS 02-1098), and the (200) plane appeared at 44.39° for Au and at 44.51° for Ag. From these results, it can be confirmed that the nanoparticles deposited on the ESM contain both Ag and Au.

3.3 Raman studies

Raman spectroscopy is highly useful to characterize disulphides and thiols present in ESM, because the Raman bands are more intense compared to their infrared absorption bands. Since ESM contains keratin having disulphide bonds, we used Raman spectroscopy to characterize the ESM and metal immobilized ESM. In Fig. 5d the Raman spectra of the bare ESM and metal
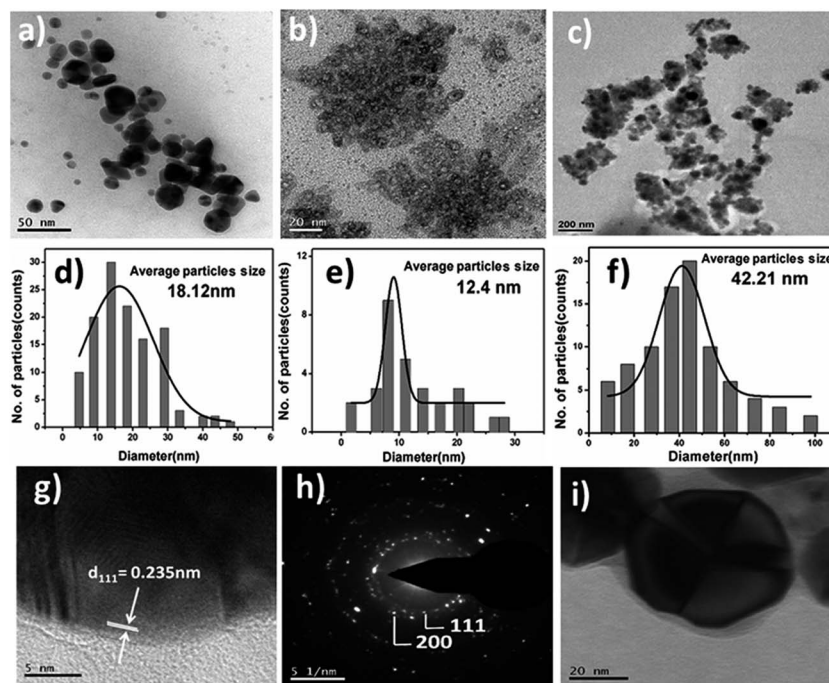
Fig. 4 TEM images of (a) Au, (b) Ag, and (c) AuAg alloy NPs. Particle size distribution of (d) Au, (e) Ag and (f) AuAg alloy. (g) and (h) represent the HRTEM image and SAED pattern of the AuAg alloy and (i) is TEM image of a single particle of the AuAg alloy.

nanoparticle incorporated ESM are presented. Several peaks were observed in normal ESM, which were tentatively assigned to the presence of various S–S, C–S and amide linkages.[29] The

weak bands at 510 and 540 cm^{-1} correspond to the presence of S–S stretching bonds, confirming the presence of disulphide bonds, the band at 756 cm^{-1} corresponds to C–S bonds, that at

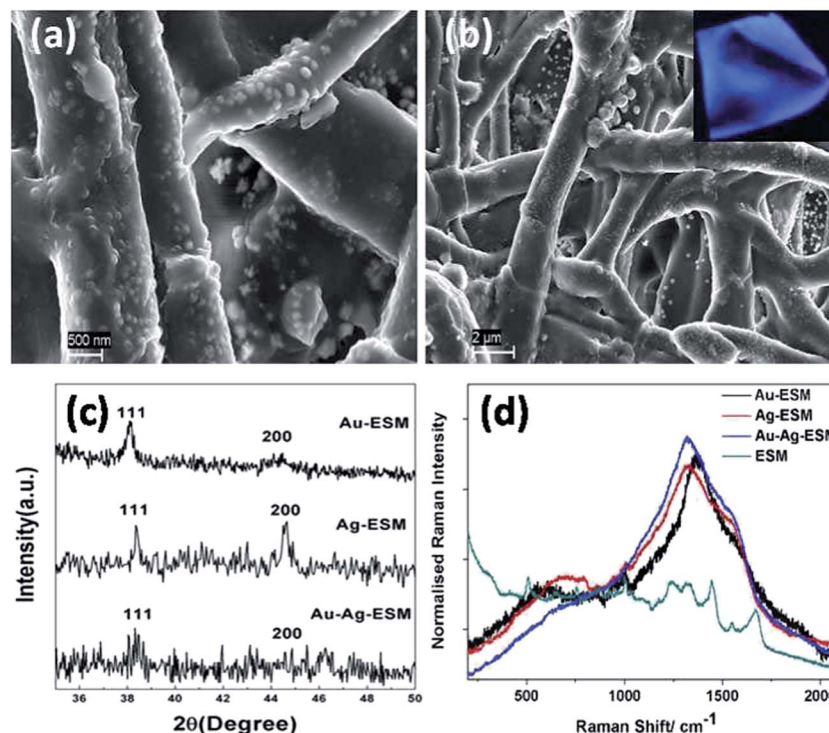**Fig. 5** (a) and (b) FESEM images of Au–Ag-ESM. (c) XRD patterns for Au-ESM, Ag-ESM and AuAg-ESM. (d) Raman spectra of normal ESM and Au, Ag, Au–Ag alloy immobilized membrane. The inset image shows the blue-emitting AuAg-ESM membrane under UV light.

1450 cm^{-1} corresponds to C–H bonds, and many smaller and weaker stretching bands at 1247, 1335, 1460, 154 and 1660 cm^{-1} correspond to various amide linkages present in the ESM.[28] It is highly interesting to notice the dramatic change in the Raman intensity of the ESM resulting in a broad band in the 1000–1700 cm^{-1} on deposition of the metal nanoparticles. This clearly confirms that after the reduction of metal ions the characteristic features of the ESM disappear. The new broad peaks appeared at 1360 cm^{-1}, 1316 cm^{-1} and 1322 cm^{-1}, respectively, for the Au-ESM, Ag-ESM and AuAg-ESM. The intensity was highest for AuAg-ESM upon 785 nm laser excitation for 10 s. The change in the intensity of these bonds could possibly be associated with changes in the functional groups of the proteins present on the ESM as a result of the deposition of metal ions. This could also give an indication of the reaction of various functional groups with the metal nanoparticles. Work is in progress to explore the application of these metal coated membranes for SERS applications. The ESM structure mainly contains glycoproteins, like collagen, and several amino acids, like glycine, cysteine, uronic acid, *etc*. During the reaction, metal ions (Au^{3+}, Ag^{1+}) are readily adsorbed on the porous ESM surface. The functional groups present on the proteins, such as –NH$_2$, –SH, –CHO, –OH groups, reduce the metal ions to form metal nanoparticles or alloy nanoparticles. It is interesting to note that the ESM proteins are insoluble in water and this rules out the influence of such protein molecules exhibiting fluorescence in the present case. Although each metal ion bears a different standard reduction potential, as shown below, the ESM is still capable of reducing individual metal ions simultaneously, resulting in the formation of alloy particles, as has been demonstrated here.

$$AuCl_4^- + 3e^- \leftrightarrow Au^0, \ E^\circ = +0.99 \ V \qquad (2)$$

$$Ag^+ + e^- \leftrightarrow Ag^0, \ E^\circ = +0.80 \ V \qquad (3)$$
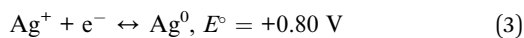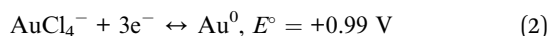
Since the reduction potential of Au$^+$/Au is higher than that of Ag$^+$/Ag, Au nucleation could start in the initial phase. The *in situ* formed Au nuclei could further induce the reduction of Ag$^+$ through electron transfer, finally resulting in the simultaneous nucleation of both Au and Ag and the formation of AuAg alloy nanoparticles and clusters.

The main constituents of ESM are glycine, alanine and uronic acid, in addition to the presence of several bacteriolytic enzymes such as lysozyme and glucosaminidase. Such a structure with a number of amino, carboxyl and carbonyl functional groups on the ESM fibres could become charged under the acidic conditions of our experiments and could bring the metal ions closer to the surface *via* hydrophobic interactions or hydrogen bonding resulting in surface adsorption. Once adsorbed on the membrane, the aldehyde (–CHO) and amino (–NH$_2$) functional groups may act as reducing agents to reduce the adsorbed ions to metal nanoparticles. Our experimental observations clearly confirmed that the *in situ* reduction in the presence of ESM could, in fact, produce fluorescent Au and AuAg nanoparticles in solution without the use of any capping/reducing agent for inducing the formation of fluorescent metal

clusters. To the best of our knowledge, this is the first report confirming the formation of fluorescent AuAg alloy nanoparticles exhibiting nanosecond lifetimes by a reduction process induced by a biotemplate, such as ESM. However, the reduction process is slow due to the weak reducing power of the functional groups present in the membrane and thus it takes a longer time to complete the reduction reaction, as shown in Fig. S4.†

3.4 Application of the metal atom immobilized ESM as a sorbent for the removal of dyes

In order to explore the practical application of the green synthesized metal immobilized ESM, we studied the pollutant dye adsorption capability of the membranes. To monitor the dye removal capability of Au, Ag and AuAg-ESM immobilized membranes, 10 mg of the nanoparticle immobilized ESM was treated with 10 ml of 10^{-5} M sodium 4-[(4-dimethylamino) phenylazo]benzene sulphonate (commonly known as Methyl Orange (MO) dye) solution in the dark. We chose the anionic dye, MO, in anticipation of the interaction of the dye molecules with the functional groups present on the surface of ESM and on the charged nanoparticles. The reaction was monitored by measuring the change in the absorbance maxima (λ_{max}) of the dye around 464 nm. Soon after the addition of the membrane to the dye solution, a bathochromic shift in the λ_{max} was observed, as evident in Fig. 6a–c. The bathochromic shift was highest in presence of Au-ESM where the absorption maxima shifted 20 nm towards the higher wavelength. No further shift in the peak position was noticed with time, except the initial peak shift. However, as evident from the absorption spectra, a systematic decrease in the intensity was noticed, indicating the adsorption of dye molecules on the membrane. Interestingly, the Au-ESM exhibited the highest adsorption capacity among the investigated membranes. The observed bathochromic shift is mainly attributed to the change in the pH of the solution. The pH of the initial MO solution in double-distilled water was 6.9, which changed to 3.4, 3.89 and 3.56 soon after the addition (5 minutes) of Au-ESM, Ag-ESM and AuAg-ESM, respectively. Along with changes in pH, the colour of the MO solution changed from yellow for the initial solution to orange after the addition of the membrane (inset of Fig. 6a–c, (1)). Finally, the adsorption gets saturated after 24 hours resulting in complete discolouration of the dye solution. The digital image (2) is the reaction media after 24 hours exhibiting a colourless solution, which is indicative of a complete adsorption of the dye molecules on the membrane. The sequential decrease in the concentration of the dye is clearly observed from the C_t/C_0 *vs.* time (Fig. 6d) plot. From Fig. 6e, it can be observed that the % dye removal capability of the Au-ESM is the maximum (90.43%), followed by Ag-ESM (82%) and AuAg-ESM (80.26%). In order to confirm the enhanced dye adsorption property of the Au, Ag and AuAg nanoparticle immobilized ESM, we also performed the same experiments with bare ESM. Interestingly, even after 24 hours of immobilization also, only 10.53% of the MO dye was adsorbed (Fig. 6f) on the bare ESM compared to a 90% dye adsorption on Au-ESM. Although ESM has been reported to act
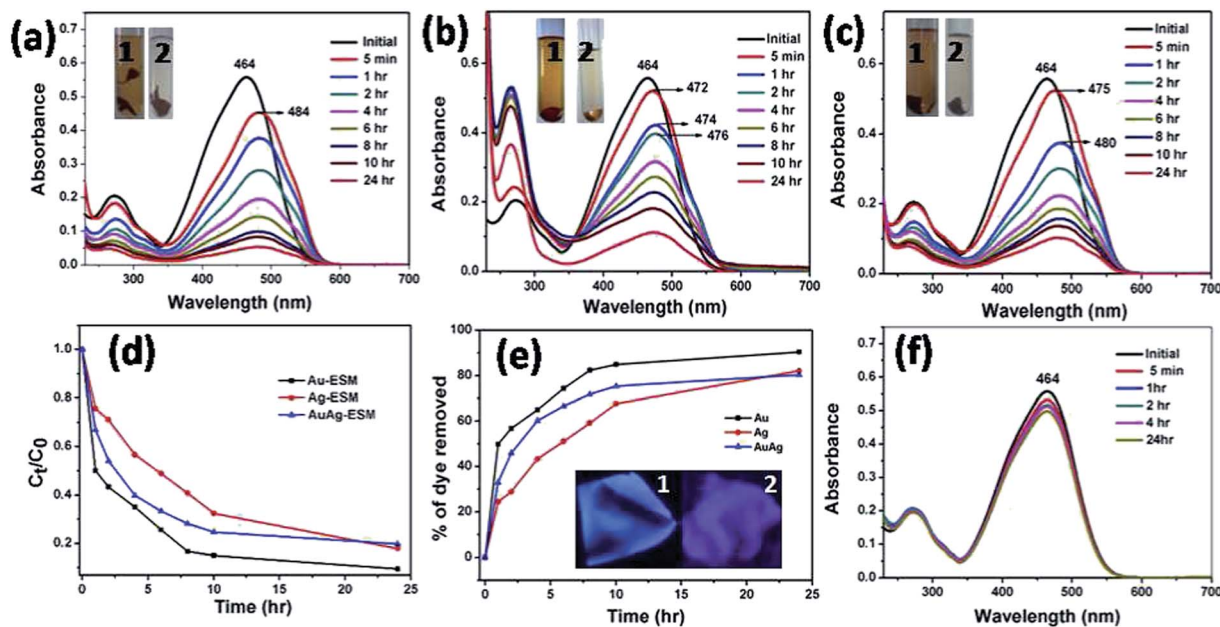
Fig. 6 (a), (b), (c) represent the absorption spectra of the MO dye solution in the presence of Au-ESM, Ag-ESM, AuAg-ESM, respectively; inset in each case shows images of the MO dye solution just after 5 minutes (1) and the dye solution after 24 h (2). (d) C_t/C_0 values of MO in the presence of the membrane, (e) % of dye removed from each of the Au, Ag and AuAg ESMs; inset in (e), (1) and (2) are the images of the AuAg-ESM membrane in the presence of UV light before and after dye adsorption. (f) Absorption spectra of MO in the presence of bare ESM confirms a poor adsorption.

as an adsorbent material for direct red and acid blue dyes,[30] for anionic dyes, like MO, it exhibited very poor adsorption characteristics. We also carried out the experiments in a phosphate buffer solution of pH ∼7. In the buffer solution also, the metal nanoparticle immobilized ESM exhibited good adsorption properties, which is evident from the reduction in the absorbance of MO at 464 nm (Fig. S14†). However, the adsorption was higher in distilled water compared to that in the buffer solution.

We also treated the metal nanoparticle immobilized ESM with a cationic dye (Methyl Violet) under similar experimental conditions. Interestingly, no dye adsorption was observed with MV dye molecules, as evident from the absorbance data shown in the ESI (Fig. S15†). Interaction of the particle dispersion with the dye was also extremely poor, with no change in the dye absorbance, except a minor shift in the λ_{max} position (Fig. S16†). Although the metal nanoparticles were reported to be active in enhancing the degradation of MO,[31] in our case we anticipated an enhanced adsorption of the dye molecules on the ESM in the presence of the metal nanoparticles. In order to prove that this is not a catalytic degradation, we carried out desorption studies with the MO adsorbed membranes. After completion of the dye adsorption, metal nanocluster immobilized ESMs were taken out and dried at RT. The dried membranes were added to a 0.005 M NaOH solution to study the dye desorption experiments. During this process the colour of the solution changed from colourless to yellow and the characteristic absorbance peak intensity of MO in solution gradually increased. This is because the desorption of the anionic dye molecules adsorbed on the nanocluster immobilized ESM released them to the solution. The desorption was completed within two hours. The

data for the desorption experiments are presented in Fig. S17.† In Fig. 7, the percentage adsorption and desorption are compared in a bar diagram. Almost 88.2% of the adsorbed dye molecule were desorbed from Au-ESM whereas for AuAg-ESM and Ag-ESM the desorption rate was only 74% and 68.38%, respectively. A minimum amount of the dye still remained adsorbed on the ESM substrates probably due to their stronger interaction with the metal nanoparticles. A schematic of the interaction between a metal nanoparticle immobilized ESM and MO dye is presented in Fig. 8. Our experiments with this naturally occurring biomembrane confirmed that a metal ion incorporated ESM could be a cost effective, eco-friendly and safe material to remove pollutant dyes from waste water.
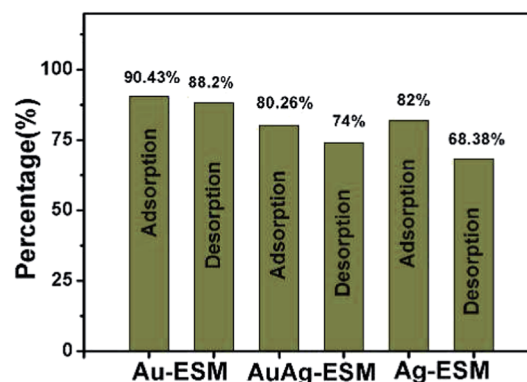

Fig. 7 Percentage of the dye adsorbed and desorped by the Au-ESM, AuAg-ESM and Ag-ESM membranes.
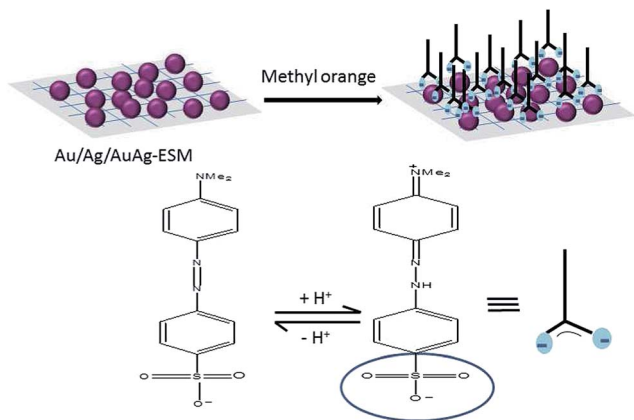
Fig. 8 Schematic of the interaction of metal nanocluster-ESM and the MO dye molecule.

4. Conclusions

The ESM mediated route has led to the formation of AuAg nanoclusters with a distinct fluorescence that could have a tremendous impact on biomedical applications. To the best of our knowledge, this is the first report on the formation of fluorescent alloy nanoparticles by the *in situ* reduction of metal ions using a naturally and abundantly available biotemplate without the use of any catalyst or chemical reducing agent at ambient conditions. We also explored the capability of these metal particle immobilized inexpensive ESMs in removing organic anionic dyes from water. The ESMs without nanoparticles were not effective in dye adsorption. These results confirm that it is the enhanced adsorption of the dye molecules in the presence of metal particles that has helped to convert ESM into an effective platform for water purification. This process has the dual advantage of utilizing the inexpensive and abundant food waste ESM for immobilizing the metal nanoparticles and at the same time using the same as an effective platform for the removal of organic dyes from water.

Acknowledgements

References

1 C. N. R. Rao, G. U. Kulkarni, P. J. Thomas and P. E. Edwards, *Chem. Soc. Rev.*, 2000, **29**, 27–35.

2 M. C. Daniel and D. Astruc, *Chem. Rev.*, 2004, **104**, 293–346.

3 Z. Luo, K. Zheng and J. Xie, *Chem. Commun.*, 2014, **50**, 5143–5155.

4 S. Zeng, D. Baillargeat, H. P. Ho and K. T. Yong, *Chem. Soc. Rev.*, 2014, **43**, 3426–3442.

5 X. Yang, L. Yang, Y. Dou and S. Zhu, *J. Mater. Chem. C*, 2013, **1**, 6748–6751.

6 J. Xie, Y. Zheng and J. Y. Ying, *J. Am. Chem. Soc.*, 2009, **131**, 888–889.

7 C. Guo and J. Irudayaraj, *Anal. Chem.*, 2011, **83**, 2883–2889.

8 A. V. Singh, B. M. Bandgar, M. Kasture, B. L. V. Prasad and M. Sastry, *J. Mater. Chem.*, 2005, **15**, 5115–5121.

9 C. L. Liu, H. T. Wu, Y. H. Hsiao, C. W. Lai, C. W. Shih, Y. K. Peng, K. C. Tang, H. W. Chang, Y. C. Chien, J. K. Hsiao, J. T. Cheng and P. T. Chou, *Angew. Chem., Int. Ed.*, 2011, **50**, 7056–7060.

10 J. S. Mohanty, P. L. Xavier, K. Chaudhari, M. S. Bootharaju, N. Goswami, S. K. Pal and T. Pradeep, *Nanoscale*, 2012, **4**, 4255–4262.

11 R. Gui and H. Jin, *Analyst*, 2013, **138**, 7197–7205.

12 P. S. Devi, S. Banerjee, S. R. Chowdhury and G. S. Kumar, *RSC Adv.*, 2012, **2**, 11578–11585.

13 M. Balaz, *Acta Biomater.*, 2014, **10**, 3827–3843.

14 M. Wong, M. J. C. Hendrix, K. von der Mark, C. Little and R. Stern, *Dev. Biol.*, 1984, **104**, 28–36.

15 J. L. Arias, M. S. Fernandez, J. E. Dennis and A. I. Caplan, *Connect. Tissue Res.*, 1991, **26**, 37–45.

16 N. Li, L. N. Niu, Y. P. Qi, C. K. Y. Yiu, H. Ryou, D. D. Arola, J. H. Chen, D. H. Pashley and F. R. Tay, *Biomaterials*, 2011, **32**, 8743–8752.

17 C. Shao, B. Yuan, H. Wang, Q. Zhou, Y. Li, Y. Guan and Z. Deng, *J. Mater. Chem.*, 2011, **21**, 2863–2866.

18 M. Liang, R. Su, R. Huang, W. Qi, Y. Yu, L. Wang and Z. He, *ACS Appl. Mater. Interfaces*, 2014, **6**, 4638–4649.

19 Q. Dong, H. Su, D. Zhang, Z. Liu and Y. Lai, *Microporous Mesoporous Mater.*, 2007, **98**, 344–351.

20 B. Zheng, L. Qian, H. Yuan, D. Xiao, X. Yang, M. C. Paau and M. M. F. Choi, *Talanta*, 2010, **82**, 177–183.

21 P. Y. Lin, C. W. Hsieh, P. C. Tsai and S. Hsieh, *ChemPhysChem*, 2014, **15**, 1577–1580.

22 R. M. Rezaei, H. Razmi and S. D. Reyhan, *Colloids Surf., B*, 2014, **118**, 188–193.

23 R. Mallampati and S. Valiyaveettil, *ACS Sustainable Chem. Eng.*, 2014, **2**, 855–859.

24 R. Shoji, T. Miyazaki, T. Niinou, M. Kato and H. Ishii, *J. Mater. Cycles Waste Manage.*, 2004, **6**, 142–146.

25 X. Zhang, M. Guo, D. Wo, P. Liu, Y. Sun, L. Zhang, Y. She, Q. Liu and F. Fan, *Int. J. Mol. Sci.*, 2011, **12**, 2972–2981.

26 X. Dou, X. Yuan, Y. Yu, Z. Luo, Q. Yao, D. T. Leong and J. Xie, *Nanoscale*, 2014, **6**, 157–161.

27 A. Kumar, P. K. Vemula, P. M. Ajayan and G. John, *Nat. Mater.*, 2008, **7**, 236–241.

28 S. K. Das, A. R. Das and A. K. Guha, *Langmuir*, 2009, **25**, 8192–8199.

29 S. J. Hamodrakas, E. L. Kamitsos and A. Papaaikolaeu, *Int. J. Biol. Macromol.*, 1984, **6**, 333–336.

30 M. Arami, N. Y. Limaee and N. M. Mahmoodi, *Chemosphere*, 2006, **65**, 1999–2008.

31 N. Gupta, H. P. Singh and R. K. Sharma, *J. Mol. Catal. A: Chem.*, 2011, **335**, 248–252.